Journal of Electroanalytical Chemistry 858 (2020) 113806

Contents lists available at ScienceDirect

Journal of Electroanalytical Chemistry

journal homepage: www.elsevier.com/locate/jelechem

γ-Fe2O3 nanoparticles anchored in MWCNT hybrids as efficient sulfur hosts for high-performance lithium-sulfur battery cathode

Jeongyeon Lee [a,1], Youngmoo Jeon [b,1], Jiseop Oh [b], Myungjin Kim [b], Lawrence Yoon Suk Lee [a], Yuanzhe Piao [b,c,*]

[a] Department of Applied Biology and Chemical Technology and the State Key Laboratory of Chemical Biology and Drug Discovery, The Hong Kong Polytechnic University, Hung Hom, Kowloon, Hong Kong

[b] Program in Nano Science and Technology, Graduate School of Convergence Science and Technology, Seoul National University, 145 Gwanggyo-ro, Yeongtong-gu, Suwon–si, Gyeonggi-do 443-270, Republic of Korea

[c] Advanced Institutes of Convergence Technology, 145 Gwanggyo-ro, Yeongtong-gu, Suwon–si, Gyeonggi-do 443-270, Republic of Korea

ARTICLE INFO

Article history:
Received 3 October 2019
Received in revised form 25 December 2019
Accepted 26 December 2019
Available online 27 December 2019

Keywords:
Iron oxide
Carbon nanotube
Refluxing reaction
Lithium-sulfur battery
Cathode

ABSTRACT

Lithium–sulfur (Li–S) battery is one of the most promising electrochemical energy storage devices due to its high energy density and reduced cost. The main challenges of Li–S battery are the severe dissolution of lithium polysulfides and low electrical conductivity of S. In this work, the synthesis of γ-Fe_2O_3 nanoparticles anchored in MWCNT (MCF) is presented through a facile method with refluxing and heating, and studied as effective S hosts in Li–S batteries. In an electrochemical analysis, the S@MCF-1 electrode shows a high rate capability (over 340 mA h g^{-1} at 7 C-rate) and stable long-term cycling performance even after 500 cycles (over 545 mA h g^{-1}, at 1 C-rate). These improved electrochemical performances could be corresponded to the two roles of γ-Fe_2O_3 nanoparticles as (1) the nodes in MWCNTs for mitigating the aggregation and volume expansion of S, and (2) the active sites and strong chemical adsorption ability on the surface of MWCNTs to directly trap polysulfides during the cycling.

1. Introduction

For large-scale energy storage applications, such as electric vehicles and energy storage systems, lithium–sulfur (Li–S) batteries have been attractive owing to their high theoretical capacity (1675 mA h g^{-1}) and energy density (2600 W h kg^{-1}) [1–6]. However, for commercialization of Li–S batteries, there are a number of obstacles, such as low S utilization, poor electrical conductivity of S (10^{-16} S m^{-1}), and volumetric expansion of S during the electrochemical reaction [7–10]. In particular, the serious shuttle effect of soluble lithium polysulfides (LiPSs) formed during repeated electrochemical reactions causes severe capacity fading [11–13]. To overcome these problems, various nanostructured carbon materials, such as hollow carbon spheres [14–16], multi-walled carbon nanotubes (MWCNTs) [17,18], and graphene nanosheet [19–21], have been studied as physical barriers and hosts for sulfur. These carbon materials not only successfully improve the deficient electrical conductivity of S but also effectively retain S due to their porous structures. However, severe capacity fading still occurs during long cycling due to the weak interactions between non-polar carbon and polar LiPSs [22]. Accordingly, many researchers have used polar metal oxides, such as TiO_2 [23,24], Fe_2O_3 [25–27], and MnO_2 [28–30], to suppress the dissolution of the LiPSs by chemical interaction with the polar LiPSs [31,32]. For example, Manthiram et al. reported yolk-shelled carbon@Fe_3O_4 nanoboxes for host materials in Li–S batteries, and they showed that the polar Fe_3O_4 cores could effectively trap the LiPSs by strong chemical interaction, resulting in highly enhanced performances [33]. Zhang et al. presented a trapping effect of LiPSs with oxygen defected-TiO_2 nanosheets in Li–S batteries [34].

Herein, we introduce a facile synthesis of γ-Fe_2O_3 nanoparticles anchored in multi-wall carbon nanotube (MWCNT) hybrids as efficient S hosts for Li–S batteries. The hybrids of the γ-Fe_2O_3 nanoparticles anchored in MWCNT (MCF) provides porous carbon networks with a high electrical conductivity to retain the sulfur in MWCNTs, which allows a rapid path for electrons and Li-ions during the electrochemical reactions. In addition, the anchored γ-Fe_2O_3 nanoparticles also serve as active sites to directly trap polysulfides during the cycling. As a result, the S@MCF-1 electrode

* Corresponding author at: Program in Nano Science and Technology, Graduate School of Convergence Science and Technology, Seoul National University, 145 Gwanggyo-ro, Yeongtong-gu, Suwon–si, Gyeonggi-do 443-270, Republic of Korea.
E-mail address: parkat9@snu.ac.kr. (Y. Piao).

[1] These authors contributed equally to this work.

http://dx.doi.org/10.1016/j.jelechem.2019.113806

shows a high rate capability and stable long-term cycling performance even after 500 cycles.

2. Experimental

2.1. Chemicals

MWCNT was purchased from CNT Co., Ltd. Iron(III) nitrate nonahydrate ($Fe(NO_3)_3{\cdot}9H_2O$, 98.5%) and nitric acid (HNO_3, 68–70%) were purchased from Samchun Co. All reagents were used without further purification.

2.2. Synthesis of γ-Fe_2O_3/MWCNT (MCF) hybrids

At first, 0.1 g of MWCNTs and 0.5 g of iron(III) nitrate nonahydrate ($Fe(NO_3)_3{\cdot}9H_2O$, 98.5%) were dispersed in 40 mL of concentrated nitric acid solution with ultrasonication for 1 h. Then, the mixture was refluxed at 100 °C for 9 h with continuous stirring and naturally cooled to RT. The product was collected by centrifugation and washed with DI water and ethanol for several times, and freeze-dried overnight. Subsequently, the product was heated with a heating rate of 10 °C min^{-1} to 400 °C and maintain at that temperature for 8 h in a tube furnace under Ar atmosphere. The as-obtained γ-Fe_2O_3/MWCNT powders were dispersed in DI water by ultrasonication for 1 h to remove any contaminants. Finally, γ-Fe_2O_3/MWCNT hybrids (MCF-1) were collected using a membrane filter and washed with DI water and ethanol for several times. The obtained MCF-1 was fully dried in a vacuum oven.

For comparison, 0.1 g of MWCNTs and 1.0 g of iron(III) nitrate nonahydrate ($Fe(NO_3)_3{\cdot}9H_2O$, 98.5%) were used to prepare MCF-2 hybrids (MCF-2) with the same experimental conditions.

2.3. Synthesis of S@γ-Fe_2O_3/MWCNT (S@MCF) composite

S@γ-Fe_2O_3/MWCNT composites were obtained by the typical melting diffusion method. The as-prepared MCF-1 and MCF-2 samples were thoroughly mixed with S in a mortar (weight ratio of MCF:S, 3:7), respectively. The mixed powder was then heated at 155 °C for 12 h in a tube furnace under an Ar atmosphere. Then, these products were further heated at 200 °C for 30 min to remove the S on the surface of MCFs.

2.4. Preparation of Li_2S_6 solution

Li_2S_6 solution was prepared by dissolving elemental S and lithium sulfide (Li_2S) (molar ratio of 5:1) in a mixed solvent of 1,2-dimethoxyethane and 1,3-dioxolane (DME/DOL, with a volume ratio of 1:1) with vigorous stirring at 50 °C for 24 h in an Ar-filled glove box.

2.5. Material characterization

The morphology was characterized by using field emission scanning electron microscopy (FESEM, Hitachi S-4800) and high-resolution transmission electron microscopy (HRTEM, JEOL JEM-2010) with an energy dispersive X-ray (EDX) spectrometer to detect the elemental signals. X-ray diffraction (XRD) patterns were obtained using an X-ray diffractometer (D8-Advance) with Cu Kα (λ = 1.5406 Å) radiation. The weight ratios of S, iron oxide and carbon in the composite were measured using thermogravimetric analysis (TGA/DSC 1, Mettler Toledo Co.) in a nitrogen or air atmosphere from RT to 600 °C at a heating rate of 10 °C min^{-1}. N_2 adsorption-desorption isotherms were obtained using an adsorption analyzer (BELSORP-mini II). Raman analysis was performed with a Raman spectrometer (HORIBA Scientific-T64000) using a 514.5 nm laser source.

2.6. Electrochemical characterization

The S composite, Super P, and poly(vinylidene fluoride) (PVDF) in *N*-methyl pyrrolidone (NMP) were mixed by ball milling (Mini-Mill Pulverisette 23, Fritsch) in a weight ratio of 7:2:1 to form a homogeneous slurry and then casted onto a pure aluminum foil by a doctor blade with a thickness of 100 μm. The electrode was dried in an oven at 60 °C for 12 h to remove the NMP solvent and cut by a punching machine with a diameter of 11 mm. The loading density of the active material was from 0.98 to 1.02 mg cm^{-2}. CR2016 coin cells were assembled in an argon-filled glove box with moisture and oxygen contents below 1 ppm. The Li metal foil and Celgard 2400 were used as the counter electrode and the separator, respectively. The electrolyte was prepared by dissolving 1.0 M bis (trifluoromethane)sulfonamide lithium salt (LiTFSI) and 1 wt% $LiNO_3$ in a mixed solvent of 1,2-dimethoxyethane and 1,3-dioxolane (DME/DOL, with a volume ratio of 1:1), and 30 μL of electrolyte was used in each coin cell. The galvanostatic charge/discharge tests were performed on a WBSC3000s cycler (WonATech, Korea) at different current densities with a voltage window of 1.7–2.8 V versus Li^+/Li. The cyclic voltammetric (CV) test was conducted at a scan rate of 0.1 mV s^{-1} with a voltage window of 1.7–2.8 V versus Li^+/Li. Electrochemical impedance spectroscopy (EIS) analysis was measured in the frequency range of 0.1–100 kHz.

3. Results and discussion

Fig. 1 illustrates the synthetic process for the S@MCF-1 prepared by a wet chemical process and loaded sulfur by a melt diffusion method. $Fe(NO_3)_3$ solutions with MWCNT were refluxed at 100 °C for 9 h and then continuously stirred at RT. Fe precursors can penetrate into the cavity of MWCNT via capillary forces and attach on the outside of MWCNT (Fig. 1 #2). After that, the material was separated by centrifugation and dried using a freezing dryer. Then, the material was heated at 400 °C for 8 h in Ar as shown in Fig. 1 #3. For the infiltration of S in the composite, the as-prepared 16% of γ-Fe_2O_3 nanoparticle-anchored MWCNT (MCF-1) and S were homogeneously mixed and heated at 155 °C for 12 h under an Ar atmosphere (Fig. 1 #4).

Fig. 2a and b show the SEM images of MCF-1 and S@MCF-1, respectively. The SEM image of MCF-1 (Fig. 2a) shows the typical shape of MWCNT and a hollow structure, while that of S@MCF-1 (Fig. 2b) shows the S-infiltrated MCF-1 without any aggregation of S. Additionally, Fig. S1 shows the SEM images of MWCNT (Fig. S1a and b) and MCF-2 (Fig. S1c and d) at low and high magnification. Due to the small size, it is difficult to distinguish the existence of nano-sized γ-Fe_2O_3 dots from Fig. 2 and S1. XRD analysis was performed to determine the structures of the samples as shown in Fig. 2c and Fig. S2. Fig. 2c shows the XRD patterns of pristine S, MCF-1, and S@MCF-1. Compared to the XRD patterns of MC, those of MCF-1 and MCF-2 indicate iron oxide patterns (red dots in Fig. 2c and Fig. S2), which are assigned to γ-Fe_2O_3 (PDF: 39-1346) [35,36]. In Fig. S2, the patterns for MC, MCF-1, and MCF-2 show the broadened diffraction peaks at 26.5 and 43.2°, which correspond to the (002) and (004) planes of graphitic carbon (JCPDS 75-1621) [37]. Thermogravimetric analysis (TGA) was performed to confirm the actual S contents in S@MC, S@MCF-1, and S@MCF-2, respectively. In Fig. 2d, a sharp decrease in weight was observed in the range of 200 to 300 °C, indicating the removal of S. The actual S contents in S@MCF-1, S@MCF-2, and S@MC were calculated to be 65%.

To confirm the γ-Fe_2O_3 contents in MC, MCF-1, and MCF-2, TGA analysis in Fig. S3 was conducted under air atmosphere. The contents of γ-Fe_2O_3 in MCF-1 and MCF-2 were calculated to be 16 and 32 wt%, respectively. N_2 adsorption-desorption isotherms were analyzed to obtain the surface area and pore volumes as shown in Fig. S4 and Table S1, respectively. MC, MCF-1, and MCF-2 showed the surface areas of 278.48, 258.55, and 201.81 $m^2 g^{-1}$ and total pore volumes of 1.31, 1.91, and 1.07 $cm^3 g^{-1}$, respectively. After the impregnation of S into these samples by melt diffusion, the surface areas of S@MC, S@MCF-1, and S@MCF-2 are significantly reduced, corresponding to the impregnation of S into the pores of MC, MCF-1, and MCF-2. MCF-2 shows the lowest surface areas among these samples.

To further investigate the morphology and composition of the samples, TEM analysis with EDX mapping was conducted, as shown in Fig. 3 and

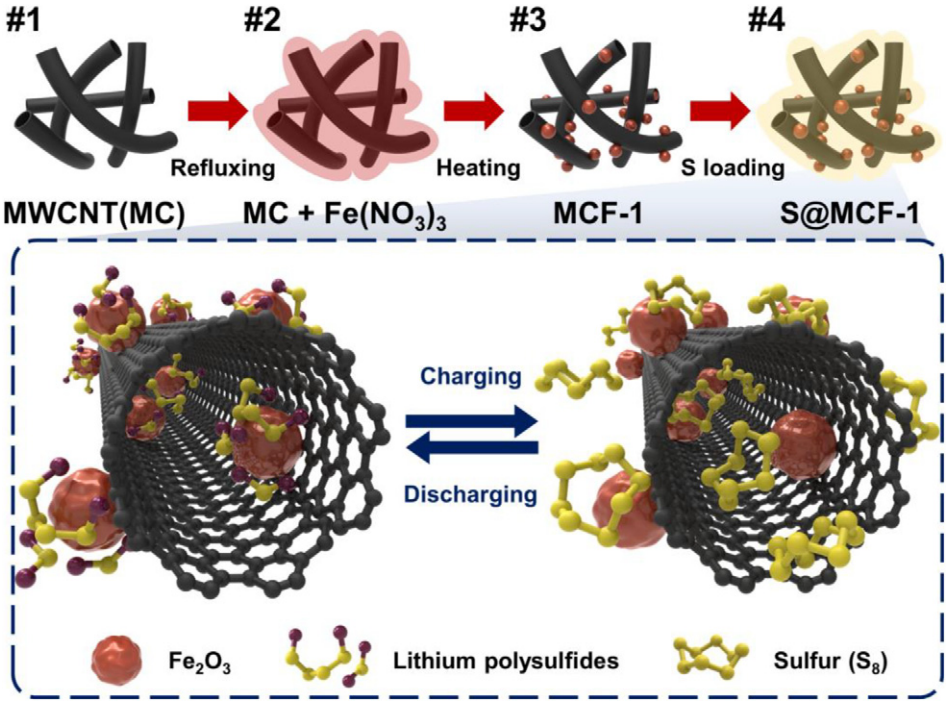

Fig. 1. Schematic representation of the synthesis and the discharging/charging process of S@MCF-1.

Fig. S5. In Fig. 3a and b, MCF-1 shows the typical MWCNT with γ-Fe_2O_3 dots on both inside and outside of MWCNT. For comparison with MCF-1, the TEM image of MCF-2 in Fig. S5b showed the excess γ-Fe_2O_3 dots on MWCNT with even aggregation of γ-Fe_2O_3, indicating the lowest pore volumes. To observe the composition of the samples, X-ray photoelectron spectroscopy (XPS) analysis of the S@MCF-1 is conducted, as shown in Fig. 4. In Fig. 4a, there are C, O, Fe, and S elements in the full scan, respectively. In the C 1s region, the XPS spectra display binding energies at approximately 284.7, 286.5, and 288.2 eV, which correspond to C–C, C–O, and C–O–C bonds, respectively. For the O 1s, there are three peaks with binding energies of approximately 530.4, 531.7, and 533.3 eV, which can be assigned to O–Fe, O–C, and O–H, respectively. Additionally, in the Fe 2p region, it shows Fe $2p_{1/2}$ and Fe $2p_{2/3}$ at approximately 725.3 and 711.6 eV, which are for γ-Fe_2O_3 [38]. As shown by the XRD, EDX mapping, and XPS

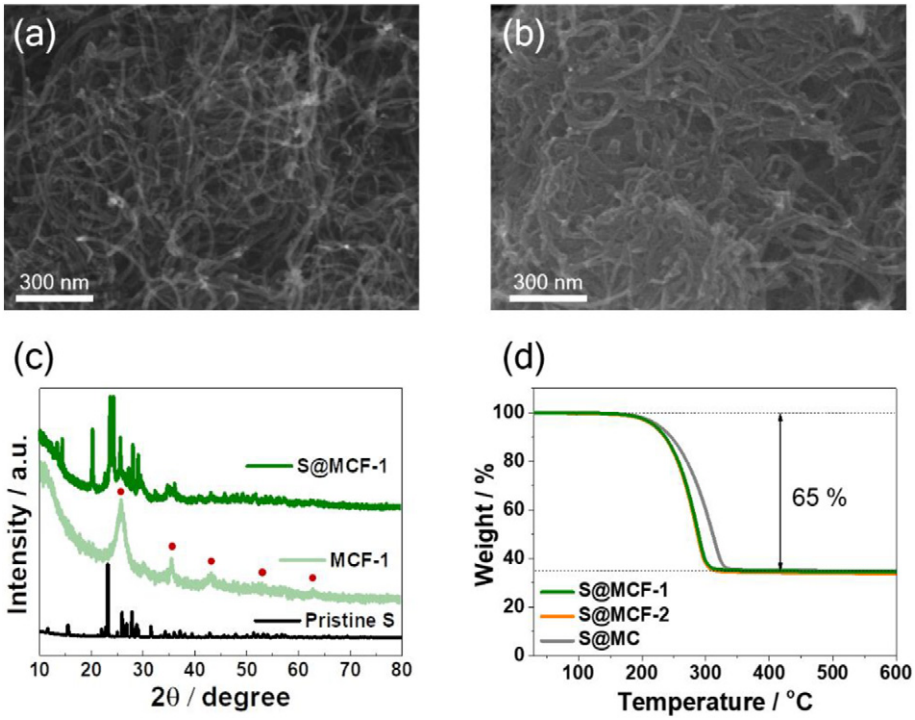

Fig. 2. SEM images of (a) MCF-1 and (b) S@MCF-1; (c) XRD patterns of S@MCF-1, MCF-1, and pristine S; (d) TGA analysis of S@MCF-1, S@MCF-2, and S@MC.

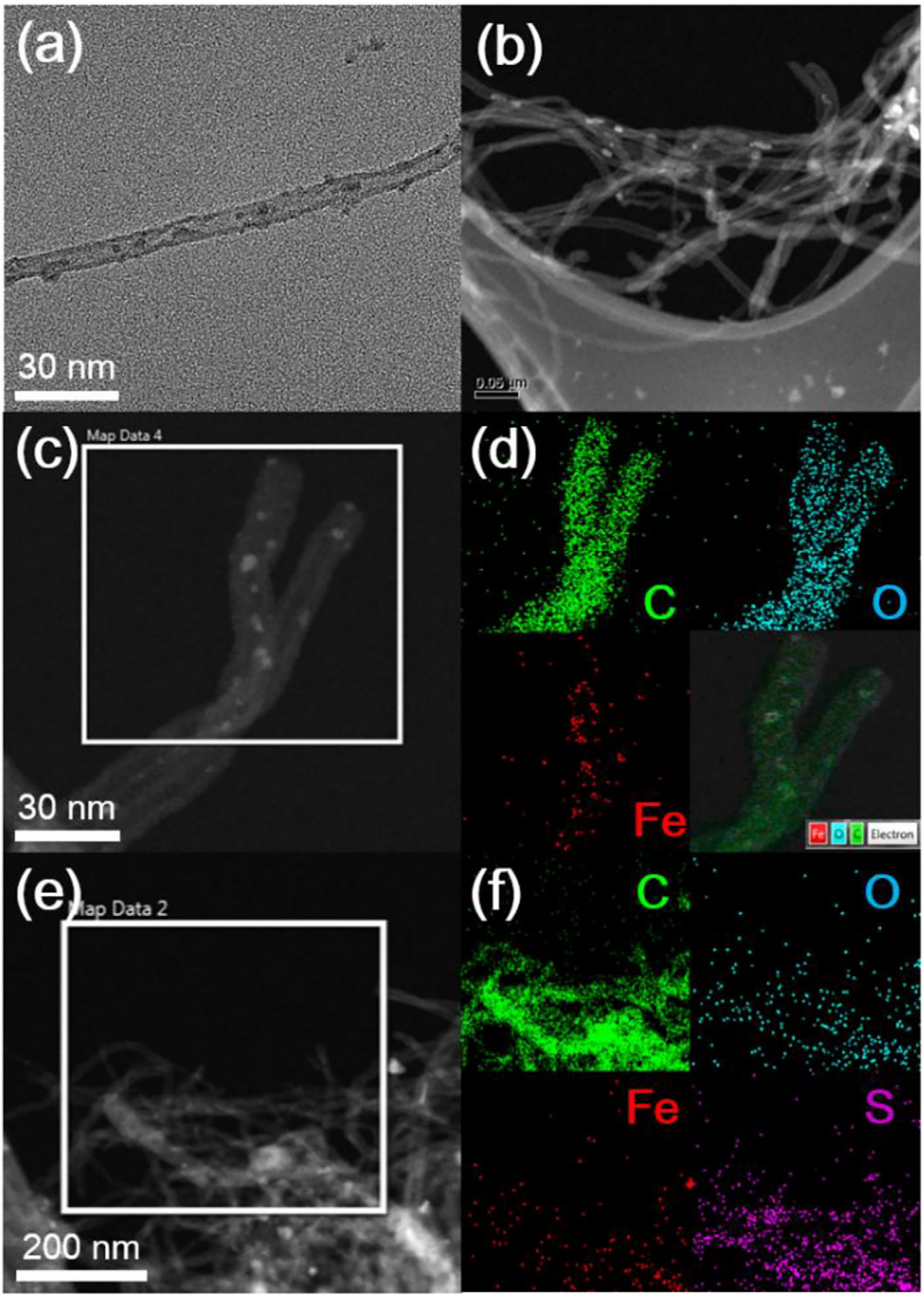

Fig. 3. TEM images of (a, b) MCF-1 and EDX mapping results of C, O, Fe, and S for (c, d) MCF-1 and (e, f) S@MCF-1.

analysis, γ-Fe_2O_3 nanoparticles are well attached on the MWCNT. We expect that these γ-Fe_2O_3 nanoparticles in and outside of the MWCNT can trap the polysulfides during cycling. To investigate the electrochemical performance, we conducted the galvanostatic charge/discharge profiles and cyclic voltammetry (CV) tests, as shown in Fig. 5. The charge/discharge profiles of the S@MCF-1 electrode in Fig. 5a were tested at a current density of 0.1 (1 and 2 cycles) and 1.0 C-rate (3 to 100 cycles), respectively. Despite the partial dissolution of LiPSs observed during the initial 2 cycles with a low current density, the S@MCF-1 electrode showed a specific capacity of 1208.7 mA h g^{-1} and 1113.5 mA h g^{-1} at the 1st and 2nd cycles, respectively. Moreover, the S@MCF-1 electrode showed excellent cycling stability over 100 cycles (1 C-rate), indicating the strong chemical adsorption between LiPSs and γ-Fe_2O_3 nanoparticles on the MWCNT.

Fig. 5b shows the CV curves of the S@MCF-1 electrode during 5 cycles at 0.1 mV s^{-1} in the voltage range of 1.7–2.8 V. The CV curves of S@MCF-1 show two cathodic peaks at approximately 2.3 and 2.1 V, which are

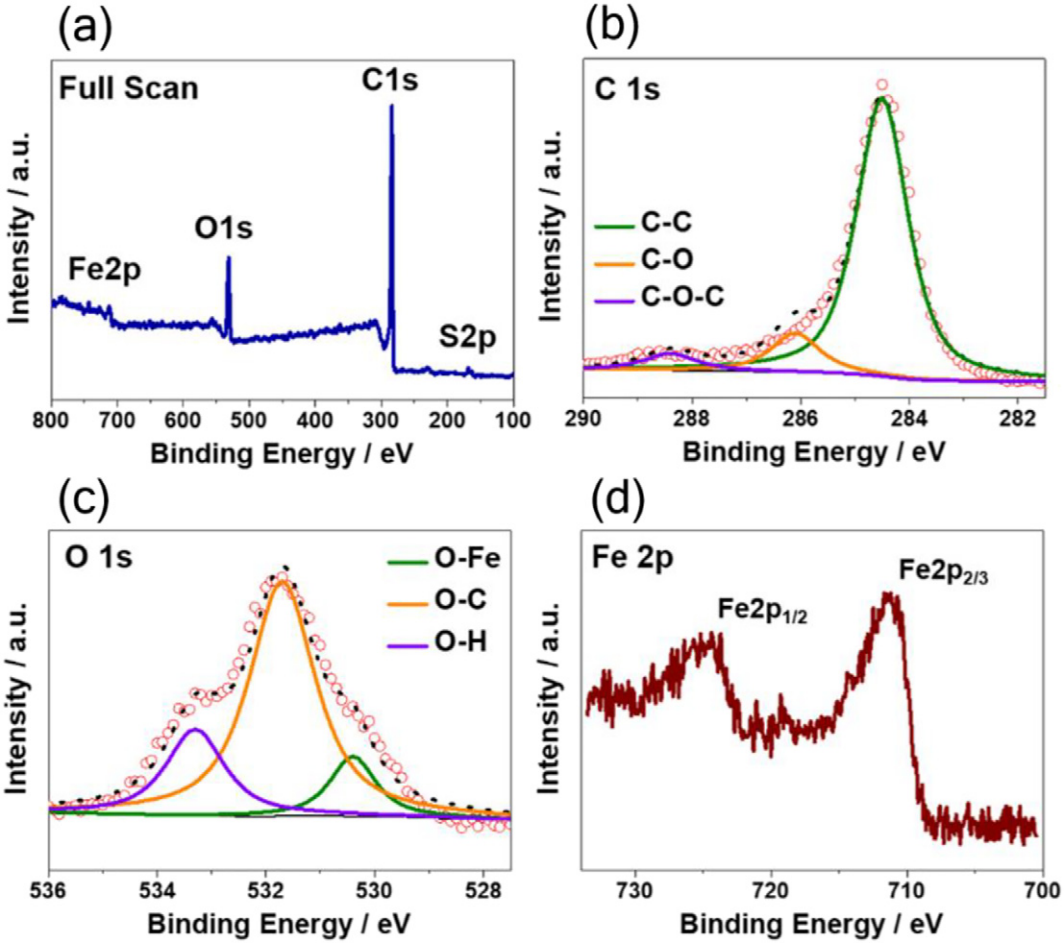

Fig. 4. XPS spectrum of S@MCF-1: (a) full scan, (b) C 1s, (c) O 1s, and (d) Fe 2p.

assigned to the reduction of S to polysulfides with long chains (Li_2S_n, $4 \leq n \leq 8$) and the further reduction of polysulfides with long chains to insoluble polysulfides with short chains (Li_2S_n, $n \leq 2$), respectively [39]. The anodic peak at approximately 2.4 V corresponds to the reversible oxidation of polysulfides to S. The peak shifts are not observed in the S@MCF-1 electrode during 5 cycles, indicating a highly stable cyclability. As shown in Fig. 6a, the cycle performances of S@MC, S@MCF-1, and S@MCF-2 electrodes were conducted at 1 C-rate over 100 cycles. Compared with S@MCF-1 and S@MCF-2 electrodes, faster capacity fading were observed on S@MC electrode. Rate capability tests for S@MC, S@MCF-1, and S@MCF-2 electrodes were also conducted as shown in Fig. 6b. Among these electrodes, S@MCF-1 electrode shows the highest specific capacity. These results show that the loading amount of γ-Fe_2O_3 strongly effect the electrochemical performances of the composite material. Fig. 6c shows the long-term cycling performance of S@MCF-1 electrode (545.6 mA h g^{-1} at the 500th cycle at 1 C-rate), resulting from the effective carbon network and optimized γ-Fe_2O_3 nanoparticles loading. Furthermore, the electrode of S@MCF-1 with high loading (2 mg cm^{-2}) (Fig. S6) retains a specific capacity of over 400 mA h g^{-1} after 100 cycles.

To confirm the effect of γ-Fe_2O_3 nanoparticles in MWCNT on chemical adsorption with polysulfides, we conducted a polysulfide adsorption test with host materials (MC and MCF-1) and Li_2S_6 solution. Initial visual observation Li_2S_6 solution and MC and MCF-1 in Li_2S_6 solutions is shown in Fig. S7. For each sample, 10 mg of MC and MCF-1 was put into 10 mL of 50 mM Li_2S_6 solutions. These samples were sonicated for 1 h and placed in a glove box for 12 h without further shaking. After 12 h (Fig. 7a), the Li_2S_6 solution with MCF-1 turned colorless, but the other showed a yellow color, corresponding that it was difficult to trap the polysulfides with only MC. Furthermore, ultraviolet-visible (UV–vis) spectroscopy was used to determine the degree of chemical affinity between the host materials and polysulfides. UV–vis measurements of the clear upper remnants of MC and MCF-1 in Li_2S_6 solutions after aged for 12 h were performed, as shown in Fig. 7b. The UV–vis spectroscopy results (Fig. 7b) indicate that the absorption peak of Li_2S_6 solution with MCF-1 at approximately 400–450 nm (a visible light region) nearly disappeared, while that of Li_2S_6 solution with MC only slightly decreased compared to the peak for the Li_2S_6 solution. These results indicate that γ-Fe_2O_3 nanoparticles in MWCNT strongly trap polysulfides, resulting in excellent electrochemical performances. Fig. S8 shows the SEM images of the S@MC and S@MCF-1 electrodes over 100 cycles. Like Li_2S_6 adsorption and the UV–vis spectra, the 100 cycled S@MC electrode in Fig. S8a shows excess agglomeration and rough surfaces, which were caused by the severe dissolution of LiPSs compared to that of S@MCF-1 in Fig. S8b.

Fig. S9 showed visual observation of the separators for (a) S@MC and (b) S@MCF-1 electrodes after 100 cycles. The separator of the S@MC cell (Fig. S9a) exhibited more severe dissolution of LiPSs and a thicker yellow color, compared to that of S@MCF-1 (Fig. S9b), which is correspondence with the results of the UV–vis spectroscopy measurements. As shown in Fig. 7c and d, EIS analysis of the S@MCF-1 and S@MCF-2 electrodes before and after cycling was performed to compare their charge transfer resistances (R_{ct}), which are shown by the depressed semicircles in the upper-frequency region. As shown in

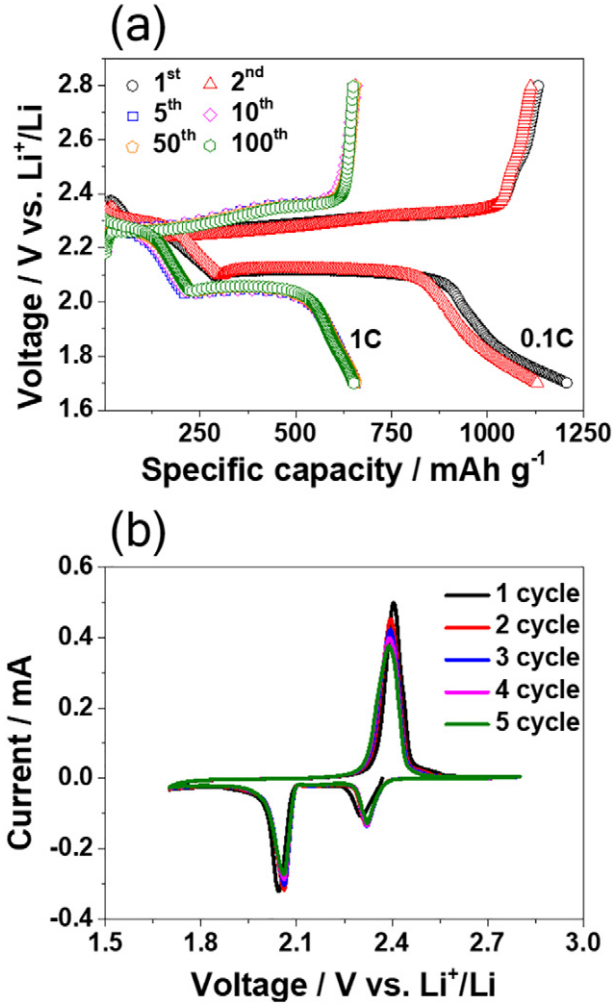

Fig. 5. (a) Galvanostatic charge/discharge profiles of the S@MCF-1 electrode at current densities of 0.1 C-rate (1 and 2 cycles) and 1.0 C-rate (3 to 100 cycles). (b) CV curves for the S@MCF-1 electrode in voltage range of 1.7 to 2.8 V.

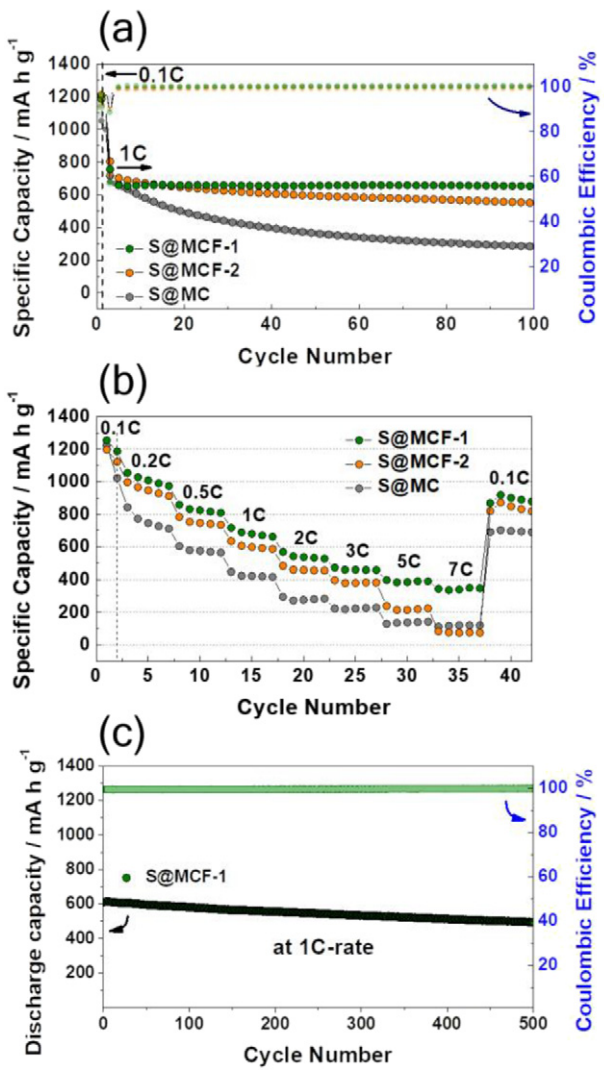

Fig. 6. (a) The cycling performance of S@MC, S@MCF-2, and S@MCF-1 electrodes at 1 C-rate for 100 cycles. (b) Rate performances of the S@MC, S@MCF-2, and S@MCF-1 electrodes with various current densities (0.1 to 7.0 C-rate). (c) Long-term cycle performance of the S@MCF-1 electrode at 1 C-rate for 500 cycles.

Fig. 7c, the S@MCF-1 electrode had a slightly lower R_{ct} before cycling than the S@MCF-2 electrodes. After 100 cycles, the S@MCF-1 electrode also had a smaller R_{ct} than that of S@MCF-2, as shown in Fig. 7d. These results also support that the reasonable ratio of γ-Fe_2O_3 nanoparticles to carbon networks results in the superior electrochemical performances for Li–S batteries.

4. Conclusion

In this work, we report the synthesis of γ-Fe_2O_3 nanoparticles-anchored MWCNT hybrid materials for S hosts in Li–S batteries. γ-Fe_2O_3 nanoparticles in the composites provided nodes in the MWCNTs for good dispersion of S in the composites and active sites to efficiently trap the polysulfides during cycling. The γ-Fe_2O_3 nanoparticle/MWCNT composites exhibited a high rate capability (over 340 mA h g^{-1} at 7 C-rate) and stable long-term cycling performance even after 500 cycles (over 545 mA h g^{-1}, at 1 C-rate). Various analysis, such as Li_2S_6 adsorption test, UV–vis spectroscopy measurements, SEM images of the cycled electrodes, and photos of the cycled separators were made to support the improved electrochemical performances of S@MCF-1 cell. Hence, our study indicates that the γ-Fe_2O_3 nanoparticle/MWCNT composites are promising host materials for Li–S batteries.

CRediT authorship contribution statement

Jeongyeon Lee: Conceptualization, Data curation, Formal analysis, Software, Writing - original draft. **Youngmoo Jeon:** Conceptualization, Data curation, Formal analysis, Software, Writing - original draft. **Jiseop Oh:** Data curation, Formal analysis. **Youngmoo Jeon:** Data curation, Formal analysis.**Lawrence Yoon Suk Lee:** Funding acquisition, Methodology, Project administration, Resources, Validation, Visualization. **Yuanzhe Piao:** Formal analysis, Funding acquisition, Methodology, Project administration, Resources, Supervision, Validation, Visualization.

Acknowledgements

This work was supported by the Basic Science Research Program through the National Research Foundation of Korea (NRF) funded by the Ministry of Education (NRF-2018R1D1A1B07051249), Nano Material Technology Development Program (NRF-2015M3A7B6027970) and Science and Technology Amicable Relationships (STAR) Program (NRF-2019K1A3A1A21031052) of MSIT/NRF. This work was also supported by the Center for Integrated Smart Sensors funded by the Ministry of

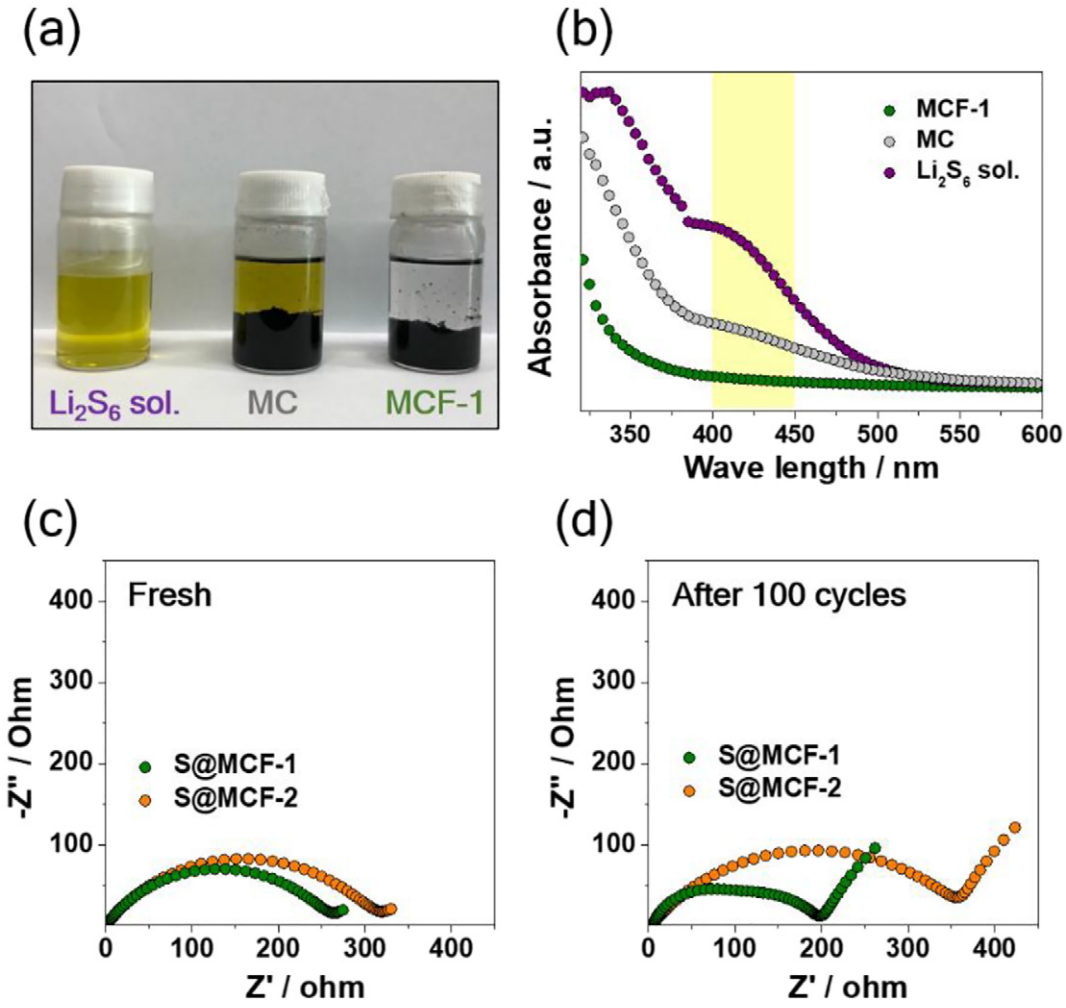

Fig. 7. (a) Visual observation of the Li_2S_6 solution, MC, and MCF-1 in the Li_2S_6 solutions after 12 h. (b) UV–vis spectroscopy results of Li_2S_6 solution, MC, and MCF-1 after 12 h. EIS spectra of (c) fresh cells and (d) 100 cycled cells for S@MCF-1 and S@MCF-2.

Science, ICT and Future Planning, Republic of Korea, as Global Frontier Project (CISS-2012M3A6A6054186).

Appendix A. Supplementary data

Supplementary data to this article can be found online at https://doi.org/10.1016/j.jelechem.2019.113806.

References

[1] M. Armand, J.M. Tarascon, Nature 451 (2008) 652–657.
[2] B. Dunn, H. Kamath, J.M. Tarascon, Science 334 (2011) 928–935.
[3] B. Scrosati, J. Hassoun, Y.K. Sun Energ, Environ. Sci. 4 (2011) 3287–3295.
[4] N.S. Choi, Z.H. Chen, S.A. Freunberger, X.L. Ji, Y.K. Sun, K. Amine, G. Yushin, L.F. Nazar, J. Cho, P.G. Bruce, Angew. Chem. Int. Edit. 51 (2012) 9994–10024.
[5] P.G. Bruce, S.A. Freunberger, L.J. Hardwick, J.M. Tarascon, Nat. Mater. 11 (2012) 19–29.
[6] J. Kim, D.J. Lee, H.G. Jung, Y.K. Sun, J. Hassoun, B. Scrosati, Adv. Funct. Mater. 23 (2013) 1076–1080.
[7] Y. Yang, G.Y. Zheng, Y. Cui, Chem. Soc. Rev. 42 (2013) 3018–3032.
[8] M. Wild, L. O'Neill, T. Zhang, R. Purkayastha, G. Minton, M. Marinescu, G.J. Offer, Energy Environ. Sci. 8 (2015) 3477–3494.
[9] A. Manthiram, S.H. Chung, C.X. Zu, Adv. Mater. 27 (2015) 1980–2006.
[10] S. Urbonaite, T. Poux, P. Novak, Adv. Energ. Mater. 5 (2015), 1500118.
[11] D.A. Boyd, Angew. Chem. Int. Edit. 55 (2016) 15486–15502.
[12] D.W. Wang, Q.C. Zeng, G.M. Zhou, L.C. Yin, F. Li, H.M. Cheng, I.R. Gentle, G.Q.M. Lu, J. Mater. Chem. A 1 (2013) 9382–9394.
[13] X.L. Ji, K.T. Lee, L.F. Nazar, Nat. Mater. 8 (2009) 500–506.
[14] N. Jayaprakash, J. Shen, S.S. Moganty, A. Corona, L.A. Archer, Angew. Chem. Int. Edit. 50 (2011) 5904–5908.
[15] Y.B. An, Q.Z. Zhu, L.F. Hu, S.K. Yu, Q. Zhao, B. Xu, J. Mater. Chem. A 4 (2016) 15605–15611.
[16] Y.H. Qu, Z.A. Zhang, X.W. Wang, Y.Q. Lai, Y.X. Liu, J. Li, J. Mater. Chem. A 1 (2013) 14306–14310.
[17] J.R. He, Y.F. Chen, P.J. Li, F. Fu, Z.G. Wang, W.L. Zhang, J. Mater. Chem. A 3 (2015) 18605–18610.
[18] W. Ahn, S.N. Lim, D.U. Lee, K.B. Kim, Z.W. Chen, S.H. Yeon, J. Mater. Chem. A 3 (2015) 9461–9467.
[19] N.W. Li, M.B. Zheng, H.L. Lu, Z.B. Hu, C.F. Shen, X.F. Chang, G.B. Ji, J.M. Cao, Y. Shi, Chem. Commun. 48 (2012) 4106–4108.
[20] K. Ding, Y.K. Bu, Q. Liu, T.F. Li, K. Meng, Y.B. Wang, J. Mater. Chem. A 3 (2015) 8022–8027.
[21] X.D. Huang, B. Sun, K.F. Li, S.Q. Chen, G.X. Wang, J. Mater. Chem. A 1 (2013) 13484–13489.
[22] M.P. Yu, J.S. Ma, H.Q. Song, A.J. Wang, F.Y. Tian, Y.S. Wang, H. Qiu, R.M. Wang, Energy Environ. Sci. 9 (2016) 1495–1503.
[23] J.Y. Hwang, H.M. Kim, S.K. Lee, J.H. Lee, A. Abouimrane, M.A. Khaleel, I. Belharouak, A. Manthiram, Y.K. Sun, Adv. Energ. Mater. 6 (2016) 1501480.
[24] Y. Zhao, W. Zhu, G.Z. Chen, E.J. Cairns, J. Power Sources 327 (2016) 447–456.
[25] C.C. Zhao, C. Shen, F.X. Xin, Z.X. Sun, W.Q. Han, Mater. Lett. 137 (2014) 52–55.
[26] C. Zheng, S.Z. Niu, W. Lv, G.M. Zhou, J. Li, S.X. Fan, Y.Q. Deng, Z.Z. Pan, B.H. Li, F.Y. Kang, Q.H. Yang, Nano Energy 33 (2017) 306–312.
[27] Z.X. Cao, J.Y. Jia, S.N. Chen, H.H. Li, M. Sang, M.G. Yang, X.X. Wang, S.T. Yang, ACS Appl. Mater. Int. 11 (2019) 39772–39781.
[28] W. Sun, X.G. Ou, X.Y. Yue, Y.X. Yang, Z.H. Wang, D. Rooney, K.N. Sun, Electrochim. Acta 207 (2016) 198–206.
[29] Z. Li, J.T. Zhang, X.W. Lou, Angew. Chem. Int. Edit. 54 (2015) 12886–12890.
[30] X. Liang, L.F. Nazar, ACS Nano 10 (2016) 4192–4198.
[31] J.T. Zhang, H. Hu, Z. Li, X.W. Lou, Angew. Chem. Int. Edit. 55 (2016) 3982–3986.
[32] S.S. Zhang, D.T. Tran, J. Mater. Chem. A 4 (2016) 4371–4374.

[33] J.R. He, L. Luo, Y.F. Chen, A. Manthiram, Adv. Mater. (2017) 29.
[34] H.C. Wang, C.Y. Fan, Y.P. Zheng, X.H. Zhang, W.H. Li, S.Y. Liu, H.Z. Sun, J.P. Zhang, L.N. Sun, X.L. Wu, Chem. Eur. J. 23 (2017) 9666–9673.
[35] W.S. Ning, B. Li, B. Wang, X.Z. Yang, Y.F. Jin, Catal. Lett. 149 (2019) 431–440.
[36] K. Woo, H.J. Lee, J.P. Ahn, Y.S. Park, Adv. Mater. 15 (2003) 1761–1764.
[37] X.H. Xia, D.L. Chao, Y.Q. Zhang, J.Y. Zhan, Y. Zhong, X.L. Wang, Y.D. Wang, Z.X. Shen, J.P. Tu, H.J. Fan, Small 12 (2016) 3048–3058.
[38] X.L. Yu, S.R. Tong, M.F. Ge, J.C. Zuo, C.Y. Cao, W.G. Song, J. Mater. Chem. A 1 (2013) 959–965.
[39] A. Manthiram, Y.Z. Fu, S.H. Chung, C.X. Zu, Y.S. Su, Chem. Rev. 114 (2014) 11751–11787.